Supplementary Information: A dynamic isotope effect in the nucleophilic substitution reaction between F^- and CD_3I

Atilay Ayasli[1], Arnab Khan[†1], Thomas Gstir[1], Tim Michaelsen[1], Dóra Papp[2], Yan Wang[3,4], Hongwei Song[4], Minghui Yang[4,5], Gábor Czakó[2] and Roland Wester[1*]

[1]Institut für Ionenphysik und Angewandte Physik, Universität Innsbruck, Technikerstraße 25, 6020 Innsbruck, Austria.
[2]MTA-SZTE Lendület "Momentum" Computational Reaction Dynamics Research Group, Interdisciplinary Excellence Centre and Department of Physical Chemistry and Materials Science, Institute of Chemistry, University of Szeged, Rerrich Béla tér 1, Szeged H-6720, Hungary.
[3]School of Chemical and Environmental Engineering, Hubei Minzu University, Enshi, 445000, China.
[4]Key Laboratory of Magnetic Resonance in Biological Systems, State Key Laboratory of Magnetic Resonance and Atomic and Molecular Physics, National Center for Magnetic Resonance in Wuhan, Wuhan Institute of Physics and Mathematics, Innovation Academy for Precision Measurement Science and Technology, Chinese Academy of Sciences, Wuhan, 430071, China.
[5]Wuhan National Laboratory for Optoelectronics, Huazhong University of Science and Technology, Wuhan, 430074, China.

*Corresponding author(s). E-mail(s): roland.wester@uibk.ac.at;

[†]Present address: Department of Physics, Indian Institute of Science Education and Research (IISER) Bhopal, India

Supplementary Note 1: Assignment of reaction mechanisms from the measured scattering images

In the main text, we assign contributions of different reaction mechanisms extracted from the measured data. Here, we will briefly explain how these mechanisms were assigned and how the error is estimated.

We are able to assign the contributions of individual reaction mechanisms by cutting (velocity and angle dependent) parts in the velocity distributions associated to them. The contribution of each mechanism is then the ratio of counts inside the marked area to total counts in each distribution. The chosen angle and velocity cuts are presented in Figure 1 of the main manuscript. The assignment of different reaction mechanisms is similar to the assignment of a previous publication [1]. The velocity distributions are segmented into four different parts (F), (B), (I) and (S). Regions with forward scattered events are marked by (F), corresponding to the left side of the distributions. These are identified as forward scattering in the main text. Backscattered events correspond to the right side of the images and are marked with (B) and result from the direct rebound mechanism. Sideways scattering is marked as (S). Indirect mechanisms are marked as (I) in the differential cross-sections. These are complex mediated events with a lifetime longer than one rotational period before the complex breaks up and leads to the iodide product.

Slow product ions which might result from forward scattering, are challenging to differentiate from indirect scattering signatures, as these typically also result in slow product ions. Slow product ions in the differential cross-sections may be indirect (I) or forward scattered products (F) superimposed on top of each other. Therefore, they are marked as (I+F). To disentangle the forward contribution from indirect scattering, the regions marked as (I+F) have been divided into a left and a right hemisphere. The forward contribution in these regions can be estimated by subtracting the right hemisphere from the left, since it is assumed that isotropically scattered indirect products (I) are scattered into both hemispheres in equal parts. The indirect contribution is then estimated by doubling the amount of counts in the right side of each (I+F) hemisphere.

To estimate the uncertainty of our assignment, we varied the absolute velocity of each region in the figure by about $\pm$ 50 m/s to 80 m/s. Each marked region in the figure represents a three-dimensional volume on a Newton sphere. With this we are able to create volumes of different sizes and compare the amount of counts contained

within to our main assignment. The change in observed counts compared to our main assignment was used to estimate the uncertainty of each mechanism.

Supplementary Note 2: Details of the quantum dynamics simulations

The coordinate system

The six-dimensional model for the X + CH_3Y system employed in this study has been presented in our previous work [2]. The six-dimensional Jacobi coordinates for the F^- + CH_3I system is shown in Supplementary Figure 1. Here, **R** is the vector from the center of mass of CH_3I to F^-, which is also the z-axis of the body-fixed (BF) frame; **r** is the vector from the center of mass of CH_3 to I, which coincides with the C_{3v} symmetric axis of CH_3I. The symmetric CH stretching mode and the umbrella mode of the CH_3 group are described by scaled-polar coordinates (ρ, γ), and the rotation of CH_3I in the BF frame is described by the angles (θ, φ). The scaled-polar coordinates for the CH_3 group are defined as $\rho = \sqrt{x^2 + y^2}$ and $\gamma = \pi - \arctan(x/y)$ with $y = \sqrt{m_C/(m_C + 3m_H)}s$, where x is the distance between the atom H and the C_{3v} symmetry axis of CH_3I and s is the distance between the atom C and the center of the three H atoms.

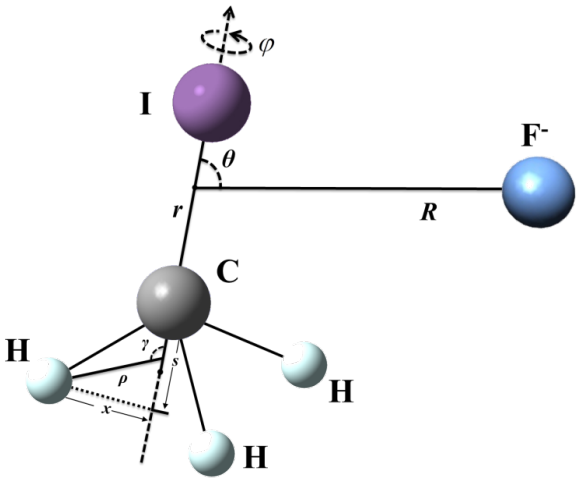

Supplementary Figure 1 The six-dimensional reactant Jacobi coordinate system for the F^- + CH_3I reaction used in the quantum dynamics calculations.

The model Hamiltonian

The 6D model Hamiltonian for the F^- + CH_3I reaction is written as ($\hbar = 1$),

$$\widehat{H} = \frac{-1}{2\mu_R}\frac{\partial^2}{\partial R^2} + \frac{\left(\widehat{J}_{\rm tot} - \widehat{J}\right)^2}{2\mu_R R^2} + \widehat{K}^{\rm vib}_{\rm CH_3I} + \widehat{K}^{\rm rot}_{\rm CH_3I} + V(R, r, \rho, \gamma, \theta, \varphi) \quad (1)$$

where μ_R is the reduced mass of the F^- + CH_3I system. $\widehat{J}_{\rm tot}$ is the total angular momentum operator of the system and $\widehat{J}$ is the rotational angular momentum operator of CH_3I. $\widehat{K}^{\rm vib}_{\rm CH_3I}$ and $\widehat{K}^{\rm rot}_{\rm CH_3I}$ are the vibrational and rotational kinetic energy operators of CH_3I, respectively. The last term $V(R, r, \rho, \gamma, \theta, \varphi)$ in the Hamiltonian is the potential energy [3].

The vibrational and the rotational kinetic operators for the CH_3I monomer defined in the (ρ, γ) coordinate system are written as,

$$\widehat{K}^{\rm vib}_{\rm CH_3I} = \frac{-1}{2\mu_r}\frac{\partial^2}{\partial r^2} - \frac{1}{2\mu_x}\left(\frac{\partial^2}{\partial \rho^2} + \frac{1}{\rho^2}\frac{\partial^2}{\partial \gamma^2} + \frac{1}{4\rho^2}\right) \quad (2)$$

where μ_r is the CH_3-I reduced mass and $\mu_x = 3m_{\rm H}$. The rotation of CH_3I is described by a rotational Hamiltonian of symmetric-top with its C_{3v} symmetric axis as the z-axis,

$$\widehat{K}^{\rm rot}_{\rm CH_3I} = \frac{1}{2I_A}\widehat{J}^2 + \left(\frac{1}{2I_C} - \frac{1}{2I_A}\right)\widehat{J}_z^2 \quad (3)$$

where $\hat{J}_z$ is the z-component of $\hat{J}$. The moments of inertia $I_{\rm A}$ and $I_{\rm C}$ are defined as,

$$I_A = \frac{m_{\rm I}\left(m_{\rm C} + 3m_H\right)}{m_{\rm I} + m_{\rm C} + 3m_{\rm H}}r^2 + \frac{3m_{\rm C}m_{\rm H}}{m_{\rm C} + 3m_{\rm H}}s^2 + \frac{3}{2}m_{\rm H}x^2 \quad (4)$$

$$I_C = 3m_{\rm H}x^2 \quad (5)$$

The time-dependent wave function is expanded in terms of the parity-adapted BF rotational basis functions $\Phi^{J_{tot}MK\varepsilon}_{Jk}$ as

$$\Psi^{J_{tot}M\varepsilon} = \sum_{n_R,n_r,n_\rho,n_\gamma}\sum_{KJk} c^{J_{tot}MK\varepsilon}_{n_R n_r n_\rho n_{\gamma Jk}}(t)\, G_{n_R}(R)\, F_{n_r}(r)\, Q_{n_\rho}(\rho)\, H_{n_\gamma}(\gamma)\, \Phi^{J_{tot}MK\varepsilon}_{Jk}\left(\widehat{R}, \widehat{r}\right) \quad (6)$$

and

$$\Phi_{Jk}^{J_{tot}MK\varepsilon} = \sqrt{\frac{1}{2\left(1+\delta_{\bar{K}0}\delta_{k0}\right)}}\left[\bar{D}_{M\bar{K}}^{J_{tot}}\bar{D}_{\bar{K}k}^{J} + \varepsilon\left(-1\right)^{J_{tot}+k}\bar{D}_{M-\bar{K}}^{J_{tot}}\bar{D}_{-\bar{K}-k}^{J}\right] \quad (7)$$

where $\bar{K} = |K|$ and ε is the parity of wavefunction under space-inverse operation. $\bar{D}_{M\bar{K}}^{J_{tot}} = \sqrt{\frac{2J_{tot}+1}{8\pi^2}}D_{MK}^{J_{tot}^*}$ and $\bar{D}_{Kk}^{J} = \sqrt{\frac{2J+1}{8\pi^2}}D_{Kk}^{J^*}$ with D_{KM}^{J} the Wigner rotation matrix. $c_{n_R n_r n_\rho n_\gamma Jk}^{J_{tot}MK\varepsilon}(t)$ are time-dependent coefficients. $G_{n_R}(R)$ are sine basis functions and the basis functions $F_{n_r}(r)$, $Q_{n_\rho}(\rho)$ and $H_{n_\gamma}(\gamma)$ are the eigenfunctions of one-dimensional reference Hamiltonians. n_R, n_r, n_ρ and n_γ are the labels for basis functions of R, r, ρ, and γ, respectively. M and K are the projections of $J_{\rm tot}$ on the space fixed (SF) and the BF z-axis, respectively. k is the projection of J on the C_{3v} symmetry axis.

The centrifugal term in the kinetic energy operator, i. e. , $(\hat{J}_{\rm tot} - \hat{J})^2$, under the centrifugal sudden (CS) approximation [4, 5] is given by

$$\left\langle \Phi_{Jk}^{J_{\rm tot}MK\epsilon} \mid (\hat{J}_{\rm tot} - \hat{J})^2 \mid \Phi_{J'k'}^{J_{\rm tot}MK'\epsilon} \right\rangle \approx \delta_{JJ'}\delta_{KK'}\delta_{kk'}[J_{\rm tot}(J_{\rm tot}+1)+J(J+1)-2K^2] \quad (8)$$

Hence, K becomes a good quantum number and is conserved under the approximation. The reaction probabilities for $J_{\rm tot} > 0$ partial waves are calculated with the CS approximation.

Propagation

The initial wave packet is constructed as the direct product of a localized wave packet $G^0(R)$ and the eigenfunction of CH_3I specified by (n_0, J_0, k_0, K_0, p_0), which represent the initial vibrational quantum number, initial rotational quantum number of CH_3I, the projection of J_0 on the C_{3v} symmetry axis, the projection of $J_{\rm tot}$ on the BF z-axis, and the parity of CH_3I, respectively. $G^0(R)$ is chosen to be a Gaussian function,

$$G^0\left(R\right) = \left(\pi\delta^2\right)^{-1/4}\exp\left[\frac{-\left(R-R_0\right)^2}{2\delta^2}\right]\exp\left(-i\sqrt{2\mu_R E_0}R\right), \quad (9)$$

where R_0 and δ are the center and width of the Gaussian function, and E_0 is the mean collision energy. The wave packet is propagated using the split operator method [6].

The reaction probability from a specific initial state is calculated by

$$P^{J_{\rm tot}\epsilon}_{n_0 J_0 k_0 K_0 p_0}(E) = \left\langle \chi_i^+ \mid \hat{F} \mid \chi_i^+ \right\rangle, \tag{10}$$

where the flux operator $\hat{F} = Im\left[\frac{1}{\mu_r}\delta(r - r^F)\frac{\partial}{\partial r}\right]$ [7]. The flux through the dividing surface, $S[r = r^F]$, is obtained from the energy-dependent scattering wavefunction, $\psi_i^+(E)$, which is computed by Fourier transforming the time-dependent wave packet at the dividing surface.

The initial state-selected integral cross section (ICS) is obtained by summing the reaction probabilities over all the partial waves (total angular momentum $J_{\rm tot}$),

$$\sigma_{n_0 J_0}(E) = \frac{1}{2J_0 + 1} \sum_{K_0 \epsilon} \left\{ \frac{\pi}{2\mu_R E} \sum_{J_{\rm tot} > K_0} (2J_{\rm tot} + 1) P^{J_{\rm tot}\epsilon}_{n_0 J_0 k_0 K_0 p_0}(E) \right\} \tag{11}$$

In this study, we focus on the dynamics from the ground ro-vibrational states, i. e. $n_0 = J_0 = 0$.

In this work, an L-shaped grid was used to reduce the size of basis set [8]. A total of 1500 sine basis functions were used for R ranging from 3.0 to 45.0 bohr and 500 grids were placed in the interaction region. 26 and 70 basis functions for r were employed in the asymptotic and interaction regions, respectively. The size of the rotational basis functions is controlled by the parameter $j_{\rm max} = 330$. Considering parity and C_{3v} symmetry, the size of rotational basis functions is 331. The size of the total basis functions is 7.27×10^8. The center of the initial wave packet is located at 40.0 bohr and the propagation time is around 6 400 000 a.u. with a time step of 20.0 a.u. The flux is taken at $r^F = 5.5$ bohr. To impose outgoing boundary conditions, negative imaginary absorbing potentials, $D(x) = -i\alpha \frac{x - x_a}{x_{\rm max} - x_a}^n$, $x_a < x < x_{\rm max}$, are applied at the grid edges of R and r. The maximum value of $J_{\rm tot}$ needed to converge the ICS is 720.

Supplementary Note 3: Integral cross section for F^- + CH_3I/CD_3I

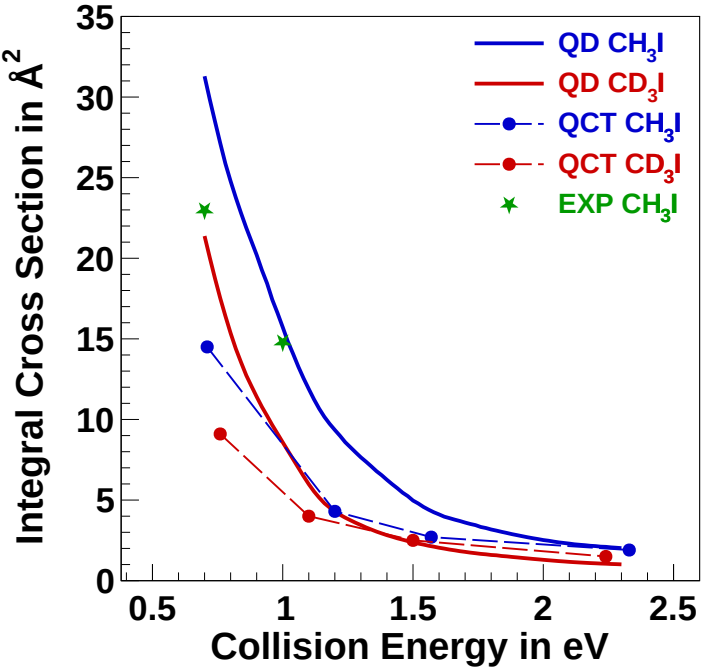

Supplementary Figure 2 Calculated integral cross sections for the hydrogenated and deuterated reactants using the QCT simulations and the quantum dynamics calculations. For comparison also two experimental values measured for CH_3I [9] have been added.

Supplementary Note 4: Stationary points for F^- + CH_3I/CD_3I

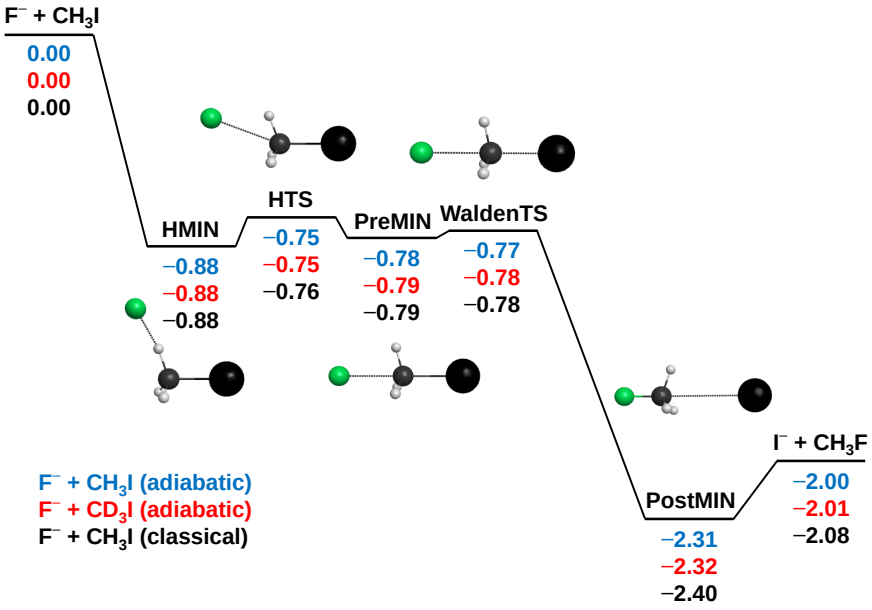

Supplementary Figure 3 Classical (clamped nuclei) and adiabatic (ZPE inclusive) relative energies (in eV) of the stationary points along the Walden-inversion pathway of the F^- + CH_3I/CD_3I S_N2 reactions on the analytical potential energy surface [3].

Supplementary Note 5: 2D scattering plots from the QCT simulations

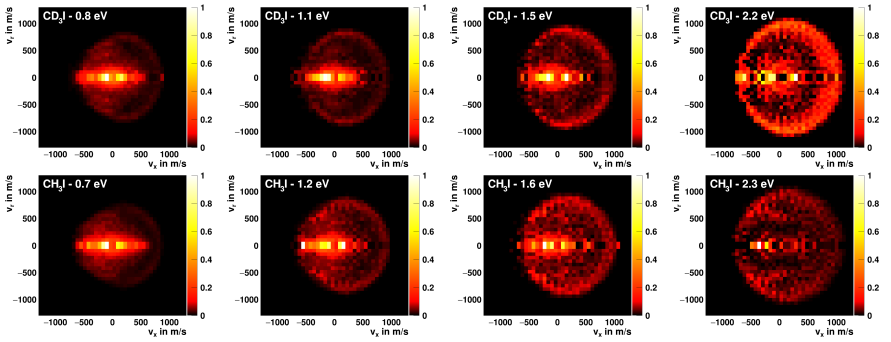

Supplementary Figure 4 Two-dimensional plots of the I^- product ion velocity in the scattering plane derived from the QCT simulations for the S_N2 channel, plotted with the same orientation as the measured velocities in figure 1 of the main text. The intensity scale shows the relative differentical cross section in arbitrary units.

References

[1] Michaelsen, T., Bastian, B., Ayasli, A., Strübin, P., Meyer, J., Wester, R.: The influence of vibrational excitation on the reaction of F^- with CH_3I: Spectator mode behavior, enhancement and suppression. J. Phys. Chem. Lett. **11**, 4331–4336 (2020). https://doi.org/10.1021/acs.jpclett.0c01095

[2] Wang, Y., Song, H., Szabó, I., Czakó, G., Guo, H., Yang, M.: Mode-specific S_N2 reaction dynamics. J. Phys. Chem. Lett. **7**(17), 3322–3327 (2016). https://doi.org/10.1021/acs.jpclett.6b01457

[3] Olasz, B., Szabó, I., Czakó, G.: High-level ab initio potential energy surface and dynamics of the F^- + CH_3I S_N2 and proton-transfer reactions. Chem. Sci. **8**(4), 3164–3170 (2017). https://doi.org/10.1039/C7SC00033B

[4] Pack, R.T.: Space-fixed vs body-fixed axes in atom-diatomic molecule scattering. sudden approximations. J. Chem. Phys. **60**, 633–639 (1974)

[5] McGuire, P., Kouri, D.J.: Quantum mechanical close coupling approach to molecular collisions. jz-conserving coupled states approximation. J. Chem. Phys. **60**, 2488–2499 (1974)

[6] Feit, M.D., Fleck, J. J. A.: Solution of the Schrödinger equation by a spectral method II: Vibrational energy levels of triatomic molecules. J. Chem. Phys. **78**, 301–308 (1983). https://doi.org/10.1063/1.444501

[7] Miller, W.H., Schwartz, S.D., Tromp, J.W.: Quantum mechanical rate constants for bimolecular reactions. J. Chem. Phys. **79**, 4889–4898 (1983)

[8] Zhang, D.H., Zhang, J.Z.H.: Accurate quantum calculation for the benchmark reaction H_2 + OH $\rightarrow$ H_2O + H in five-dimensional space: Reaction probabilities for $j = 0$. J. Chem. Phys. **99**(7), 5615–5618 (1993). https://doi.org/10.1063/1.465954

[9] Su, T., Morris, R.A., Viggiano, A.A., Paulson, J.F.: Kinetic energy and temperature dependences for the reactions of fluoride with halogenated methanes: experiment and theory. J. Phys. Chem. **94**(22), 8426–8430 (1990). https://doi.org/10.1021/j100385a014